



The performance of mesoporous magnetite zeolite nanocomposite in removing dimethyl phthalate from aquatic environments

Ehsan Ahmadi^a, Babak Kakavandi^{b,c}, Ali Azari^{a,*}, Hasan Izanloo^d, Hamed Gharibi^e, Amir Hossein Mahvi^a, Allahbakhse Javid^e, Seyed Yaser Hashemi^a

^aDepartment of Environmental Health Engineering, School of Public Health, Tehran University of Medical Sciences, P.O. Box 6446-14155, Tehran 1471613151, I.R. Iran, Tel. +98 21 88779118; Fax: +98 21 88779487; emails: ehsanahmadi_eh@yahoo.com (E. Ahmadi), Ali_Azari67@yahoo.com (A. Azari), ahmahvi@yahoo.com (A. Hossein Mahvi), s.yaser.hashemi@gmail.com (S.Y. Hashemi)

^bDepartment of Environmental Health Engineering, School of Public Health, Ahvaz Jundishapur University of Medical Sciences, Ahvaz, Iran, email: kakavandi.b@ajums.ac.ir

^cEnvironmental Technologies Research Center, Ahvaz Jundishapur University of Medical Sciences, Ahvaz, Iran

^dDepartment of Environmental Health Engineering, School of Public Health, Qom University of Medical Sciences, Qom, Iran, email: h-izanoloo@muq.ac.ir

^eDepartment of Environmental Health Engineering, School of public Health, Shahrood University of Medical Sciences, Shahrood, Iran, emails: hgharibi65@gmail.com (H. Gharibi), cavid_a@yahoo.com (A. Javid)

Received 26 August 2015; Accepted 28 March 2016

ABSTRACT

In this study, magnetic zeolite nanocomposite with an average diameter of 90–100 nm was synthesized through a chemical co-precipitation method, and used for the adsorption of dimethyl phthalate (DMP) from aqueous solution. The surface morphology of the adsorbent was characterized by scanning electron microscope, transmission electron microscopy, energy dispersive X-ray, vibrating sample magnetometer, dynamic light scattering, Brunauer, Emmett, Teller, and X-ray diffraction techniques. Batch system was followed to optimize the conditions for the removal of DMP. The adsorption experiments were carried out in terms of pH, contact time, various concentrations of DMP as well as nanocomposite, and temperature. The results showed that with increase in adsorbent dosage and contact time increased the adsorption efficiency. However, the efficiency decreased by increasing pH and initial DMP concentration. Experimental data were found to fit well with Langmuir isotherm ($R^2 > 0.981$) in all the studied temperatures. Adsorption kinetics also showed that the adsorption behavior follows the pseudo-second-order kinetic model ($R^2 > 0.996$). Besides, thermodynamic analysis demonstrated that the adsorption process occurs spontaneously and is inherently endothermic. The DMP adsorption efficiency did not change after 10 batch sorption–desorption reactions, indicating the potential application prospect of the synthesized adsorbent in real water treatment.

Keywords: Dimethyl phthalate; Magnetite zeolite nanocomposite; Modeling adsorption; Kinetics; Thermodynamic

*Corresponding author.

1. Introduction

Phthalic Acid Esters (PAEs), classified as organic compounds, are being widely used to produce various forms of polymers and plastics, including plasticizers, food packing, and personal care products [1]. Moreover, various industries such as textiles, medical equipment, ceramic, electronic, cosmetics, paper, and inks are also contributing in PAEs pollution to a large extent. The effluents of these industries may reach thousands mg/L higher than natural waters [2]. Although PAEs are of wide use in various industries, these compounds can leach out from the solid products; this is mainly due to the fact that PAEs with low molecular weight, cannot be chemically bonded to the polymers [3]. In fact, based on the conducted studies, PAEs are toxic to the aquatic environment, particularly aquatic organisms, and can directly and also indirectly jeopardize human health [4]. In addition, these compounds have been reported to be the cause of endocrine and reproductive disruption, birth defects, and cancer [5]. Among the PAEs compounds, dimethyl phthalate (DMP) is being widely used by the industries, mainly due to its high saturation solubility (4,860 mg/L), in manufacturing various products [6]. It should be noted that DMP is classified as xenobiotic and marked as an emerging pollutant [7]. It has also been reported that this compound is capable of bioaccumulation in various organs [8]. In this consideration, USEPA, Clean Water Act, and WHO classified DMP as one of the priority pollutants [9].

Several methods have been proposed to destroy and/or degrade phthalates among which aerobic and/or anaerobic biological treatment processes are the most commonly applied ones [9]. However, there are several issues regarding these processes. In fact, these biological processes are time-consuming and can hardly degrade and/or remove phthalates; besides, the final compounds resulted from applying these processes are not fully known [10]. Furthermore, it should be taken into account that biologically based treatment processes cannot efficiently remove such pollutants; in other words, phthalates contain long alkyl chains (i.e. recalcitrant compounds), which make them hard to be degraded by microorganisms [11]. In addition to the biological processes, photocatalytic techniques [12], membrane treatment (i.e. RO and NF) [13], and also various chemically based methods have been studied to find appropriate methods in removing DMP. However, the expense regarding these processes is the major disadvantage of applying them. Recently, sorption methods have been focused on due mainly to their ability to efficiently remove the pollutants at low concentrations, are easily operated, and are also cost

effective as well as sludge-free [14,15]. According to the conducted studies in this issue, Chitosan beads, Zinc Methylimidazolate Framework (ZIF) [16], graphene nanoplatelets [17], magnetic iron-carbon [18], and carbon nanotubes [19] are the most commonly adsorbents used for removing PAEs. In the present study, we investigated other compounds, which are abundantly available in Iran, to produce nanoparticles form. In this regard, Zeolites (i.e. geomaterial compounds) are cost-effective alternatives to be applied in removing and recovering organic pollutants from wastewaters [20]. The properties and characteristics of Zeolites are discussed in detail in the literature [21–23]. Although microcrystal grinding can be used to produce nanozeolite, a synthesized adsorbent produced by using this method does not efficiently work [24].

In this study, we applied hydrothermal methods under a controlled environment in terms of temperature and agitation speed to synthesize nanozeolite. The main issue in using nanozeolite in this regard is its separation after the adsorption process. In order to deal with this problem, the filtration and centrifuge methods can be applied; however, these methods are also time-consuming and require unacceptable amounts of energy. Recently, researchers have focused on the magnetic technology to facilitate the mentioned problem [14,25]. By using this technology, in fact, the time needed to easily separate the adsorbent can be significantly shortened. Magnetized sorbents can be used for removing the contaminants from water, wastewater, and gaseous effluents without producing any harmful by-products and also sludge.

The present study was aimed to synthesize a zeolite-based adsorbent with magnetic properties in order to remove DMP. Iron oxide was used as a source to induce magnetic properties into nanozeolite; and, the separation process can be carried out by using an external magnetic field. In brief, the following works were conducted in this study:

- (1) Preparing magnetic zeolite nanocomposite (MZNC) and analyzing its characteristics by scanning electron microscope (SEM), transmission electron microscopy (TEM), energy dispersive X-ray (EDX), vibrating sample magnetometer (VSM), dynamic light scattering (DLS), Brunauer, Emmett, Teller (BET), and X-ray diffraction (XRD) techniques.
- (2) Investigating the efficiency of this newly synthesized MZNC for removing DMP from the solution by considering the effects of various experimental parameters, including pH, temperature, adsorbent dose, contact time, and initial DMP concentrations.

- (3) Applying equilibrium isotherms and kinetic modeling, and also thermodynamics to further assess the adsorption of DMP in a batch system.

Furthermore, DMP removal by MZNC as an adsorbent, to the best of our knowledge, has not been reported.

2. Material and methods

2.1. Chemicals and instruments

All the applied chemicals in this study were of analytical grade. Silica fumed powder (SiO_2 at $0.007 \mu\text{m}$ size), Sodium aluminate (NaAlO_2), Ferrous sulfate heptahydrate ($\text{FeSO}_4 \cdot 7\text{H}_2\text{O}$ 99%), Ammonia (NH_3 , 35%), and Ethanol ($\text{C}_2\text{H}_5\text{OH}$, >99.0%), were purchased from Sigma-Aldrich. DMP (C_6H_4 -1, 2-(CO_2CH_3)₂, ≥99%) was purchased from Merck Co., and used to prepare DMP stock solution. To adjust the pH, we used hydrochloric acid (HCl, 35–37%) and sodium hydroxide (NaOH, 93%). The chemical structure and properties of DMP are given in Table 1.

2.2. Synthesis of MZNC

According to the applied method in a study conducted by Ansari et al. we synthesized the nanozeolite by using hydrothermal process under agitation speed and controlled temperature [24]. At first, sodium aluminate and silica fumed powder were mixed in a solution to prepare aluminosilicate gel. It should be noted that the molar ratio of $\text{Na}_2\text{O}:\text{Al}_2\text{O}_3:\text{SiO}_2:\text{H}_2\text{O}$ was regulated to 5.5:1.0:4.0:190. As a result, an aluminosilicate gel containing 5.33 g of NaOH, 2.41 g of NaAlO_2 , 3.45 g of SiO_2 , and 50 g of H_2O was prepared. The prepared aluminosilicate gel was continually shaken at 25°C for 1 d; and also, hydrothermal process was carried out using an incubator shaker at 70°C for 72 h with 250 rpm. To separate the products, a centrifuge was used; and then, we used distilled water to remove impurities from them and reach the pH to < 8. After that, we left the synthesized nanozeolite at room temperature for 1 d to dry.

In addition, Fe^{2+} ions were converted to Fe_3O_4 and loaded on the synthesized nanozeolite in accordance to the co-precipitation method [26]. In this regard, 10 g of the dried nanozeolite was added to a 3 M $\text{FeSO}_4 \cdot 7\text{H}_2\text{O}$ solution and then the mixture was heated under Nitrogen gas. Afterward, 12.5% ammonia solution was added incrementally to the above mixture and kept in an ultrasonic device for 30 min. The pH of the solution in this part of the experiment reached to 11. The Fe_3O_4 NPs (oxidation state) was prepared according to the below equation:



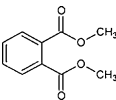
After reduction, the black beads (MZNC) were formed and separated by external magnetic field from the solution. We used distilled water and methanol to wash the beads. Then, the synthesized sorbent was dried at 60°C and stored in a desiccator.

The surface morphology of MZNC was analyzed using Scanning Electron Microscopy (SEM, S360, and Mv2300). XRD pattern was applied to study the composition crystalline structures of the nanocomposite (Quanta chrome, NOVA2000). Magnetic characteristics of MZNC were analyzed by applying VSM (Lakeshore Company, USA 7400). TEM (PHILIPS, EM 208 S 100KV), with the aim of analyzing the size and shape of the particles of composite, was also used in this work. In addition, dynamic light scattering analysis (DLC, SZ-100 nanopartica series) was used to measure the particle size distribution of nanocomposite in the solution; it is noteworthy that this process has to do with the random changes in the intensity of scattered light into the solution. Chemical characterization in order to identify the elemental composition of MZNC was performed by applying Energy-dispersive (EDX, 720/800HS).

2.3. Sorption experiments

A reactor, as shown in Fig. 1, was designed in which DMP sorption on MZNC at various temperatures (i.e. 25, 35, and 45°C) was studied. It should be mentioned that the reactor was designed to provide a batch system with 180 rpm. The DMP stock solution was prepared in DI water by which other concentrations of DMP (2–10 mg/L) solution was obtained. Considering the main variables in this process, pH (3–11), MZNC dosage (0.15–2 g/L) and contact time (0–90 min) were selected to be assessed. In addition, we used GC-MS (HP 5890 series II, Agilent, USA) to assess whether residues of DMP after the sorption process and separation of the adsorbent exist in the

Table 1
Structure and physico-chemical data for DMP

$\text{C}_{10}\text{H}_{10}\text{O}_4$ Dimethyl phthalate (DMP)	
Molecular weight (g/mol)	222.24
Henry's law constant (Pam^3/mol)	9.78×10^{-5}
Density at 20°C (Kg/m^3)	1,190

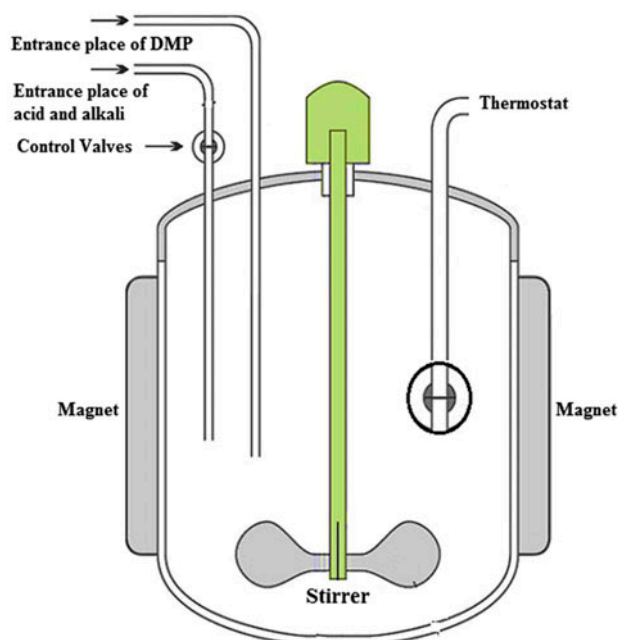


Fig. 1. Reactors designed for experiments of DMP adsorption.

solution. Specifications of GC-MS are given in Table 2. It is noteworthy that benzyl benzoate ($C_{14}H_{12}O_2$) was added to all samples as an internal standard before chromatographic analyses.

In order to ensure the reliability of the results, all the experiments were performed twice and their average values were taken as the representative of each pair of experiment. The percentage (%) of removal efficiency and adsorption capacity of DMF onto the MZNC were calculated by using the following equations:

$$\text{Removal efficiency (\%)} = 100 \times \left(1 - \frac{C_e}{C_0}\right) \quad (2)$$

$$q_e = V(C_0 - C_e)/W \quad (3)$$

Table 2
Applied GC-MS Configuration

GC	HP 5890 series II
MS	HP 5971 D
Column	DB 5 column, fused silica capillary column
ID	0.32 mm
Length	30 m
Film	1.00 μ m
Column temperature range	160–240°C
Carrier gas	Helium (31 cm/s)
Injector and detector temperatures	250–280°C

where C_0 and C_e are the initial and equilibrium concentrations of DMP (mg/L) respectively; also, q_e , V , and W stand, respectively, for the adsorption capacity (mg/g), the volume of solution (L), and weight of the required adsorbent (g).

2.4. Interfering effects of phthalate ester compounds on the sorption process

Interfering effects of common phthalate ester compounds, including DEP, DnBP, PA, DMPT, and DAP on the sorption of DMP were analyzed. In this regard, pH of the solution was adjusted in the optimal range of DMP removal. In addition, 5 g of MZNC was added in the reactor containing 8 mg/L DMP solution; and, they were mixed at 25°C with 180 rpm for 24 h. Then, the adsorbent was separated after uptake by using a magnet to determine the residual DMP.

2.5. Evaluating the reusability of MZNC

To determine the reusability of MZNC, adsorption and desorption of DMP with initial concentration of 8 mg/L was conducted ten times. It is noteworthy that the same adsorbent was used in each row of the experiments. At the end of each cycle, the DMP desorption from the surface of nanocomposite was carried out by using methanol solution at 25°C for 5 h and 250 rpm. An external magnetic field was used to separate the MZNC from the solution, and then the separated MZNC was washed several times by DI water and dried at 80°C for being used in the next adsorption–desorption cycle so as to test the reusability of nanocomposite for DMP removal. The remaining supernatant was analyzed for determining the concentration of DMP. Furthermore, the desorption percentage (%) was calculated using the following Eq. (4):

$$\text{Desorption (\%)} = \frac{C_{e(\text{des})}}{C_{e(\text{ads})}} \times 100 \quad (4)$$

3. Results and discussion

3.1. Characteristics of MZNC

The SEM, TEM, EDX, VSM, and XRD techniques were applied to determine the characteristics of the synthesized nanocomposite. Fig. 2 indicates the morphology and surface features of nanozeolite and MZNC. As shown in Fig. 2(a), the external surface of nanozeolite is rough and some pores exist on it. It also shows that these pores, with diameter of ~90 nm in average, are uniformly distributed on the surface of

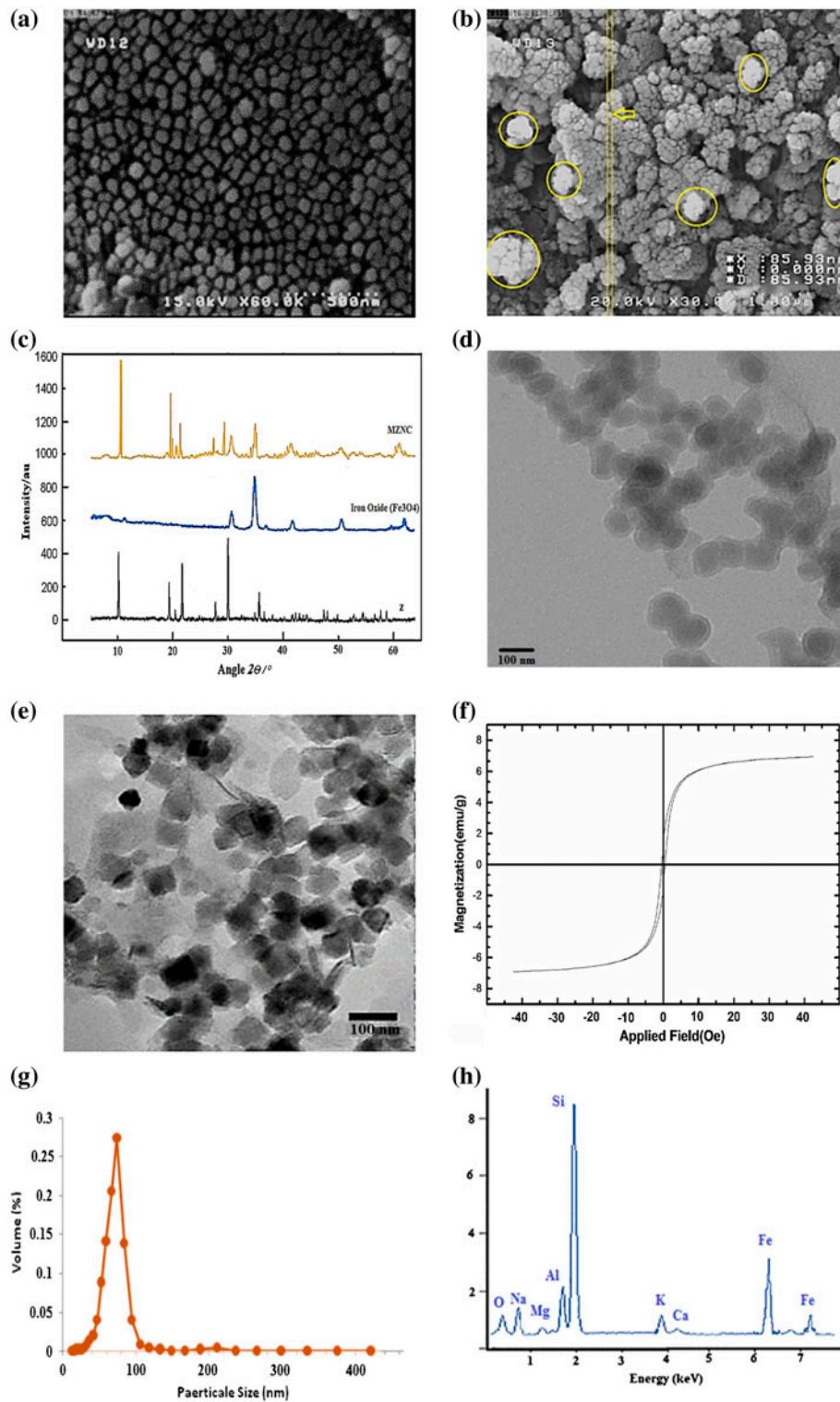


Fig. 2. SEM image of nanozeolite before (a) and after modification (b), XRD (c), TEM image of nanozeolite before (d) and after modification (e), VSM (f), DLS (g), and EDX (h) of MZNC.

nanozeolite. As can be seen from Fig. 2(b), the bright spots, which are randomly distributed on the surface of nanozeolite, represent the deposited Fe_3O_4 nanoparticles (with the mean size of 86 nm). Based on these results, it can be concluded that the zeolite and magnetite particles were successfully synthesized at nanosize scale.

X-ray diffraction patterns of nanozeolite, Fe_3O_4 particles, and MZNC in ranges of $2\theta = 5\text{--}65$ (i.e. Cu α radiation) are shown in Fig. 2(c). The XRD pattern of zeolite indicated that zeolite primarily contains heulandite ($2\theta = 10.0^\circ, 19.0^\circ, 22.7^\circ, \text{ and } 30.0^\circ$) and small amount of quartz ($2\theta = 21.0^\circ, 27.0^\circ, \text{ and } 36.5^\circ$) [20]. The peaks at $2\theta = 30.2^\circ, 35.4^\circ, 43.1^\circ, 52.4^\circ, \text{ and } 63.1^\circ$ for Fe_3O_4 particles, which were marked, respectively, by their indices (2 2 0), (3 1 1), (4 0 0), (4 2 2), and (4 4 0), indicating a cubic spinel structure of the magnetite. These peaks are consistent with those obtained from the JCPDS card No. 19-0629 for magnetite; in other words, the peaks can be taken as the indicators of the production of magnetite Fe_3O_4 [27,28]. These peaks were also observed in the pattern of synthesized MZNC, indicating that the cubic phase of Fe_3O_4 is maintained intact after the mesoporous zeolite-loading phase. Besides, related peaks to the zeolite in the patterns of MZNC were observed. X-ray diffractogram of MZNC did not show any notable change in the basic of zeolite diffraction peaks; in other words, any detectable damage to the zeolite framework not observed. Therefore, it can be concluded that the crystalline Fe_3O_4 as well as zeolite shell, and nanocomposite of MZNC were successfully synthesized. Based on the results of XRD analysis, the presence of Fe_3O_4 particles within the structure of zeolite can be assured; and also, the prepared composite can be separated from the aqueous phase by using a magnet.

By using TEM micrographs at 90 keV, as shown in Fig. 2(d) and (e), the shape and size of zeolite and magnetite particles were analyzed. In this regard, the average size of zeolite particles was found to be ~ 94 nm. The TEM micrograph of nanocomposite shows the structure of magnetite particles to be cubic with average diameter of 90–100 nm. Furthermore, the uniform distribution of the magnetite nanoparticles on the Zeolite surface can be seen from the figure.

To determine the magnetic separation ability of the sorbent, VSM technique in magnetic range of ± 10 kOe at 25°C was applied. Fig. 2(f) indicates the corresponding results. Considering the deduced curve from VSM, it was found that the maximum saturation magnetization of MZNC is 35.7 emu/g. In other words, it can be implied from this result that the adsorbent is superparamagnetic [29]. By using the VSM technique, it was also found that the magnetic nanocomposite can

be separated from the samples by applying an external magnet; it is noteworthy that this process does not lead to the formation of secondary pollutants. Dynamic light scattering particle size (DLS) analysis was carried out to determine the particle size distributions of MZNC, the results of which are indicated in Fig. 2(g). As can be seen from the figure, the narrowest obtained size distribution was ~ 86 nm, in average. This result is well in accordance with the results of SEM and TEM. By conducting EDX analysis, it was found that main elements of nanocomposite of MZNC were Si, Fe, O, Al, Na, and K; and, Mg and Ca were found in trace amounts. In addition, the amount of Si, Fe, Na, O, Al, K, Mg, and Ca atoms at the structure of Zeolite- Fe_3O_4 MNC were 34, 20, 11.1, 9.2, 13.3, 8.6, 2, and 1%, respectively. Furthermore, as shown in Fig. 2(h), the results showed that magnetite nanoparticles of iron formed on the surface of nanocomposite.

The sorbents were also analyzed by using BET technique, which the results are summarized in Table 3. The specific surface area of Nanozeolite and Iron oxide were 168–172 m^2/g , respectively. As included in Table 3, the specific surface area of MZNC (with Nanozeolite: Fe_3O_4 ratio of 2:1) was higher than other sorbents. This can be due mainly to the formation of new pores and extra surface on nanozeolite. In addition, similar findings have been reported in previously conducted studies [16]. The mean pore size of 1.84, 2.56, and 2.21 nm were recorded for nanozeolite, Fe_3O_4 nanoparticles, and MZNC 2:1, respectively. In this regard and based on the IUPAC category, all the adsorbents could be classified into mesoporous groups [30].

3.2. Effect of Fe_3O_4 MNPs loading on removal efficiency of the sorption process

The effect of MZNC molar ratio on DMP adsorption capacities was evaluated in the molar ratio of 0:1–1:0. Fig. 3(a) shows the changes of adsorption capacity in DMP by nanozeolite at different molar ratio of MZNC. It was observed that the adsorption capacity enhances when Z: Fe_3O_4 molar ratio increases from 1:0 to 2:1; but, when the Z: Fe_3O_4 molar ratios were higher than 2:1, the adsorption capacity decreased. The maximum adsorption capacity (25 mg/g) was found in the Z: Fe_3O_4 molar ratio of 2:1. Hence, this ratio was selected as the optimum state in this regard for continuing experiments with Zeolite and Fe_3O_4 nanoparticles. It is noteworthy that the values of adsorption capacity were minimum for both the Fe_3O_4 and Pure nanozeolite. Based on the results, the Zeolite and Fe_3O_4 nanoparticles synergistically affect the adsorption of DMP.

Table 3
BET analyze and average pore diameter of the MZNC

Adsorbents	Specific surface area (m ² /g)	Average pore diameter (nm)	Average pore volume (cm ³ /g)
Nanozeolite	168	1.84	0.212
4:2	171.23	1.31	0.231
2:1	188	2.56	0.291
1:1	145.74	1.21	0.232
1:2	138.32	1.65	0.245
1:4	134.24	1.92	0.259
Fe ₃ O ₄	172	2.21	0.281

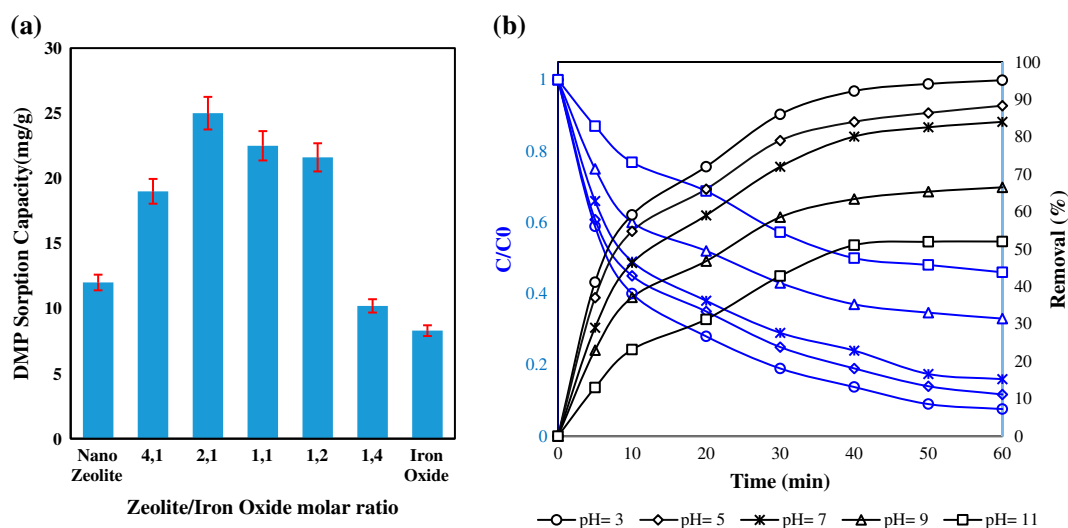


Fig. 3. (a) Effect of Z: Fe₃O₄ molar ratio on DMP adsorption. (Conditions: C₀: 10.0 mg/L, adsorbent dosage: 200 mg/L, pH 7.0 ± 0.1 and 25 ± 2 °C) and (b) effect of pH on DMP adsorption onto MZNC (Conditions: C₀: 10.0 mg/L, adsorbent dosage: 200 mg/L and 25 ± 2 °C).

3.3. Effect of pH

In this study, the effect of pH on the adsorption of DMP by MZNC for a period of 60 min was assessed, the results are shown in Fig. 3(b). It was found that when pH increases from 3 to 11, the removal percentage of DMP decreases by 42%. This result is in line with the findings of previously conducted studies on the adsorption of DMP by using different adsorbents [4]. The decrease in the adsorption of DMP with respect to the increase of pH could be due to the following reasons:

- (1) At acidic pH, surface of sorbent is protonated which in turn induces a positive charge (H⁺) on the surface. Thus, electrostatic gravity force between the positive protons and negative phenolic groups (i.e. carboxyl) of DMP could lead to the increase of adsorption efficiency [11]. At alkaline conditions, however, electrostatic

repulsion force between OH⁻ ions (Hydroxide) and negative charge of phenolic groups prevents the diffusion of DMP molecules and subsequently decreases the percentage of adsorption.

- (2) In acidic range, as shown in Fig. 4, DMP molecules ((C₂H₃O₂)₂C₆H₄) might be hydrolyzed to phthalic acid (CH(COH)). When carbonyl group from CH(COH) structure is nucleophilic, it easily reacts with hydrogen ions (H⁺) in the solution which results in the formation of positive charge by which electrostatic repulsion between MZNC and DMP improves. However, at alkaline pH, DMP molecules hydrolyze to phthalate anions, as shown in Fig. 4. In fact, the charge at surface of MZNC is of negative nature which results in having Electrostatic repulsion by which the adsorption efficiency of the process decreases.

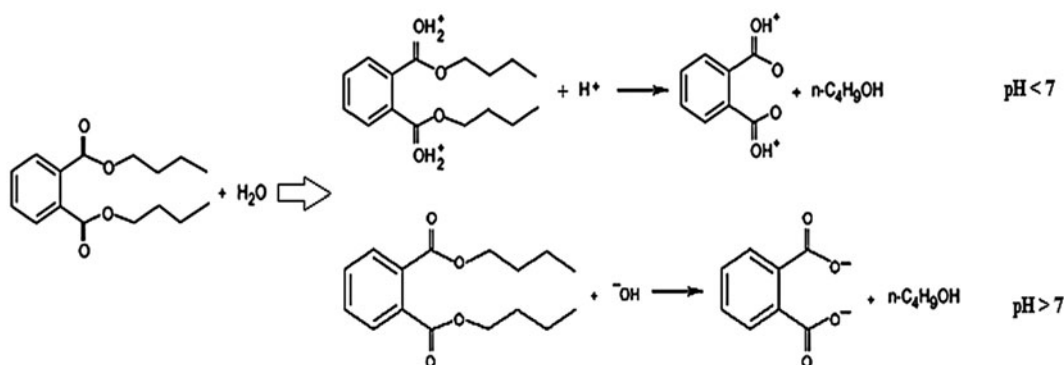


Fig. 4. DMP molecule hydrolyzes in acidic and alkaline conditions.

The surface charge of mineral oxides composite is strongly related to the pH_{pzc} of the adsorbent and also solution pH. The surface charge of the MZNC at $\text{pH} > \text{pH}_{\text{pzc}}$ is positive; and, the charge is negative when $\text{pH} < \text{pH}_{\text{pzc}}$. Moreover, pH_{pzc} can be used to determine whether the adsorption mechanism of DMP is specific or non-specific. The former type consists of ligand exchange reactions (i.e. with no significant correlation between pH and pH_{pzc}), while the coulomb forces (electrostatic attraction) play a vital role in the type of the latter one. As shown in Fig. 5(a), pH_{pzc} for the synthesized MZNC was 3.87; and also, the best DMP removal was observed at pH 3. So it can be concluded that the surface of the adsorbent is positively charged at $\text{pH} < 3.87$, which confirms the abovementioned observations made in this study. Considering the significant relationship between pH and pH_{pzc} , it can be implied that the mechanism of DPM adsorption follows a non-specific adsorption pattern.

3.4. Adsorption kinetics

In the present work, the effect of contact time, as a function of initial concentration, on the removal efficiency of DMP was studied under optimum pH; and, the results are indicated in Fig. 5(b). As can be seen from the figure, the removal rate of DMP at the first 20 min for all the studied concentrations was found to be fast; and then, the rate started gradually slowing down. Based on this result, it can be suggested that the required time to stabilize the equilibrium of the adsorption process is 20 min. The existence of ample vacant active sites on the MZNC surface is why the elimination of DMP occurs rapidly at the early stage of starting the process [31]. It is noteworthy that by increasing the contact time, the available vacant sites on the adsorbent become occupied by DMP, which contributes to the decrease of sorption rate.

In this work, the transport behavior of DMP molecules per time unit was assessed by using pseudo-first-order, pseudo-second-order, Elovich, and Intraparticle diffusion kinetic models. It should be mentioned that this assessment was conducted by applying 6 mg/L of DMP at optimized pH and over a wide range of temperatures. Regarding this issue, further details can be found at Supplementary data.

The values of correlation coefficient, R^2 , which are presented here in Table 4, were selected as a criterion to determine the best kinetic models. Considering the values of R^2 , the adsorption kinetic models for all the studied temperatures were fitted the data in the following order: pseudo-second-order > pseudo-first-order > Elovich > intraparticle diffusion. This indicates that the pseudo-second-order kinetic model describes DMP sorption on MZNC in a better way, compared with other models' descriptions of this process. In fact, this implies that the concentrations of both adsorbent and adsorbate are the rate limiting step of the adsorption process [32]. Furthermore, these results reveal that the predominant process was chemisorption, which consists of sharing or exchange of electrons between the DMP ions and the binding sites of MZNC. Some authors also reported that chemisorption is usually restricted to just one layer of molecules on the surface, although it may be followed by additional layers of physically adsorbed molecules [14,33].

In addition, the values of $q_{e,\text{Cal}}$ have a linear relationship with the temperature; in other words, DMP sorption is inherently endothermic. Arrhenius-type relationship is usually applied to calculate E_a (i.e. activation energy) using rate constant and solution temperature in the following form:

$$\ln k_2 = \ln A - \frac{E_a}{RT} \quad (5)$$

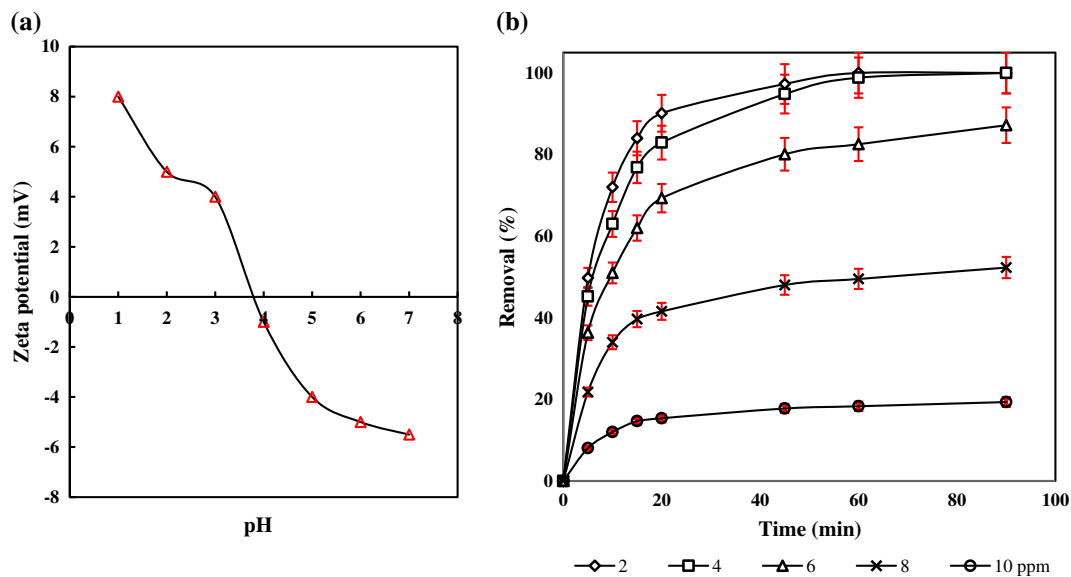


Fig. 5. (a) pH_{pzc} of MZNC and (b) effect of contact time on DMP adsorption onto MZNC (Conditions: pH 3, adsorbent dosage: 200 mg/L and 25 ± 2 °C).

Table 4
The kinetic constant values of the DMP adsorption on MZNC

Kinetic models	Temperature	Constants		
Pseudo-first-order		$q_{e,Ca1}$	K_1	R^2
	298	89.3	0.072	0.981
	308	80.01	0.067	0.987
	318	84.34	0.75	0.962
Pseudo-second-order		$q_{e,Ca1}$	K_2	R^2
	298	93.15	0.008	0.998
	308	94.52	0.012	0.999
	318	96.61	0.021	0.996
Elovich		α	β	R^2
	298	7.78	2.75	0.761
	308	7.67	2.71	0.834
	318	7.81	2.60	0.761
Intraparticle diffusion		k_i	C_i	R^2
	298	0.55	14.91	0.572
	308	0.48	14.67	0.543
	318	0.43	14.82	0.561
Experimental		$q_{e(exp)}$		
	298	92.52		
	308	93.76		
	318	95.91		

where k_2 (g/(mg min)), A , E_a (kJ/mol), R (8.314 J/mol K), and T (°K) stand for the rate constant of pseudo-second-order kinetic model, the Arrhenius

constant, the activation energy, the universal gas constant and the solution temperature, respectively. Magnitude of E_a is mainly used to understand the type of sorption which could be either physical or chemical. On one hand, physical sorption is reversible and requires low energy, ranging from 5 to 40 kJ/mol. On the other hand, chemical sorption involves stronger forces than the physical sorption; and thus, high activation energy is required (40–800 kJ/mol) [34]. The calculated activation energy at pH 3 ± 0.1 with a high regression coefficient ($R^2 > 0.99$) was 78.0 kJ/mol, which indicates that the adsorption rate of DMP on MZNC beads is controlled by the chemical process. Considering the positive values of E_a and also the favorable effect of increasing the temperature on the adsorption and adsorption processes, it can be implied that this can be inherently endothermic.

3.5. Effect of MZNC dosage

The effects of adsorbent on the adsorption efficiency were investigated at equilibrium time (20 min and the optimum pH 3) in the range of 0.5–2 g/L. Fig. 6 shows that with the increase in MZNC dosage from 0.5 to 2 g/L, the adsorption efficiency of DMP 6 mg/L increases from 16.12 to 100%. The enhancement in the adsorption can be due to increase in the adsorption surface rate, and consequently the DMP broad access to the adsorption sites on MZNC. We did not observe significant difference in the removal efficiency of 6 mg/L concentrations of DMP when the

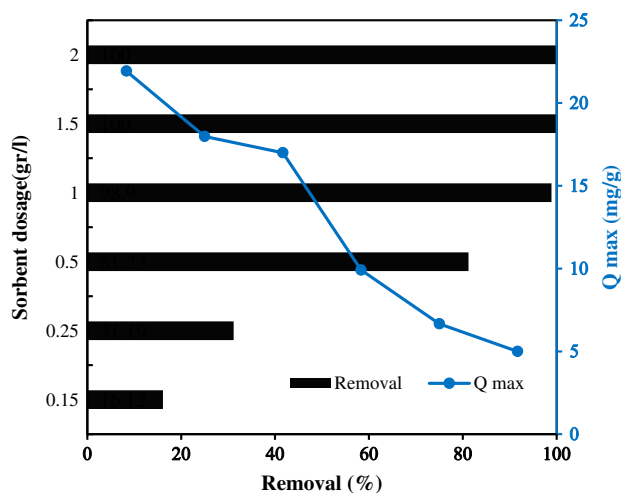


Fig. 6. Effect of MZNC dosage on DMP adsorption (Conditions: pH 3, C_0 : 6 mg/L and $25 \pm 2^\circ\text{C}$).

adsorbent dosage increased from 1 to 2 g/L. Therefore, the amount of MZNC 1 g/L was selected as optimized dosage of the adsorbent for the adsorption process. Fig. 6 also indicates that the adsorption capacity decreased dramatically from 22 to 5 mg/g when the mentioned increase in the dosage occurred. This is probably due to the split in the flux or the concentration gradient between solute concentration in the solution and the solute concentration in the surface of the adsorbent. Therefore, with increasing adsorbent mass, the amount of DMP adsorbed onto unit weight of adsorbent gets reduced causing a decrease in equilibrium adsorption density [35]. This phenomenon can also be due to the decrease of the ratio of adsorbate per mass unit of adsorbent [36]. Similar effects have been reported by previous studies [36,37].

3.6. Equilibrium isotherms

In the present study, the Langmuir, Freundlich, and Temkin isotherm models were applied to examine the experimental data with the aim of modeling the DMP sorption onto MZNC. The linear equations and parameters of adsorption equilibrium models are given in detail in the supplement Data. The adsorption isotherm experiments were conducted at pH 3 and with 2–10 mg/L of DMP; and also, the optimized adsorbent dosages at equilibrium time (20 min) and under various temperatures ($25\text{--}50 \pm 2^\circ\text{C}$) were the other factors set to model the sorption process.

As can be seen from Table 5, it was found that the values of correlation coefficients (R^2) for Langmuir, Freundlich, and Temkin models at all the studied

temperatures were >0.981 , >0.941 , and >0.939 , respectively; which, indicates that Langmuir model is the best choice for being applied to describe the DMP adsorption process. Conformity of experimental data with Langmuir isotherm represents the fact that the distribution of active sites on surface of MZNC is homogenous [38]. Furthermore, affinity of DMP toward the MZNC can be expressed by R_L parameter.

$$R_L = \frac{1}{1 + K_L C_e} \quad (6)$$

where K_L (L/mg) and C_e (mg/L) are, respectively, the Langmuir constant and the adsorbate concentration. The adsorption is favorable if the R_L happens to be between 0 and 1. The values of $R_L > 1$, $R_L = 1$, and $R_L = 0$ represent unfavorable, linear, and irreversible adsorption, respectively. As given in Table 5, the results showed that R_L values in this study are between 0 and 1, indicating that the DMP adsorption process on MZNC was favorable. This desirability of the process was also confirmed by Freundlich exponent “ n ”, since its values were $1 < n < 10$ at all the studied temperatures [39]. The values of q_m , Langmuir isotherm model, were found to be in positive correlation with the temperature of the solution. This means that the adsorption of DMP onto MZNC was an endothermic reaction in nature [14].

In order to evaluate the performance of the synthesized adsorbent in removal of DMP, we compared MZNC with other sorbent applied in the previous studies; the results are given in Table 6. Based on the results, it can be concluded that the synthesized adsorbent possesses a high sorption capacity, in comparison with the other sorbents’ capacities. Differences of the adsorption capacities of the listed adsorbents can be due to the difference in their structure, surface area, and also the properties of functional groups in each adsorbent.

3.7. Adsorption thermodynamics

Thermodynamic parameters of adsorption were determined by using K_c (distribution coefficient constant) parameters. Further details of these parameters can be found at Supplementary material. Thermodynamic parameters for the adsorption experiments of DMP on MZNC are listed in Table 7. In addition, Gibbs free energy was -3.06 , -3.91 , and -4.54 kJ/mol for 293, 308, and 323 K, respectively.

The negative values of ΔG° suggest that the adsorption of DMP on MZNC is thermodynamically

Table 5

The isothermic parameters calculated at equilibrium based on each model for the process of DMP adsorption onto MZNC

Isotherm models	Parameters	Temperature (°K)		
		293	308	323
Langmuir	q_m (mg/g)	96.026	101.23	109.52
	k_L (L/mg)	0.1377	0.33	0.41
	R^2	0.998	0.989	0.981
	R_L	0.021–0.038	0.033–0.053	0.072–0.12
Freundlich	k_f (mg/g(Lmg)/n)	4.6	4.9	5.3
	n	4	4.35	5.56
	R^2	0.973	0.951	0.941
Temkin	K_t (L/mg)	4.3	4.12	4.62
	b_t	117.06	102.45	119.06
	R^2	0.946	0.939	0.941

Table 6

Comparison of adsorption capacity of DMP between various adsorbents found in the literatures

Adsorbent	Phthalate ester	pH	Isotherm	Kinetic	q_m (mg/g)	Refs.
MZNC	DMP	3.0	Langmuir	Pseudo-second-order	109.52	This work
Magnetic poly (EGDMA-VP) beads	DEP	3.0	Langmuir and DR	Pseudo-second-order and modified Ritchie's-second-order	98.9	[40]
α -cyclodextrin-linked chitosan bead	DMP	Ineffective	Freundlich	Not done	36.48	[41]
Multiwall carbon nanotubes	DMP	5.0	Langmuir and Freundlich	Not done	62.1	[42]
Activated carbon	DEP	2.0	Freundlich	Pseudo-second-order	Not determined	[43]
Chitosan bead	DHpP	8.0	Freundlich	Pseudo-second-order	1.52	[44]
Poly (EGDMA-MATrp) beads	DEP	5.0	Langmuir	Pseudo-second-order	59.7	[45]
Magnetic iron-carbon composite	DEP	4.0	Langmuir	Pseudo-second-order	120.54	[18]
Magnetic graphene oxide	DEP	3.0	Langmuir	Pseudo-first-order	8.71	[46]
Phoenix leaves activated carbon	DBP	3.0	Freundlich	Pseudo-second-order	48.68	[47]

feasible and occurs spontaneously. Besides, the negative values of ΔG° increased by increasing the temperature; in other words, the DMP sorption could be more favorable in higher temperatures than the lower ones [14]. The ΔS° value was found to be 0.036, demonstrating that the adsorption of DMP on MZNC in solid/liquid interface randomness increases by increase in the temperature [48]. The positive value of ΔH° (10.73 kJ/mol) also suggests

that the DMP sorption process is endothermic, meaning that high temperatures can improve the sorption efficiency. As shown in Fig. 7(a), DMP adsorption percentage enhanced when the temperature increased. The maximum sorption occurred at 323°K. This indicates that DMP adsorption on MZNC is endothermic in nature, which is also in line with the results of previously conducted studies [3].

Table 7

The calculated thermodynamic parameters of the adsorption DMP on the MZNC

Temperature (°K)	Parameters		
	ΔG° (kJ/mol)	ΔH° (kJ/mol)	ΔS° (kJ/mol K)
293	-3.06	10.73	0.036
308	-3.91		
323	-4.54		

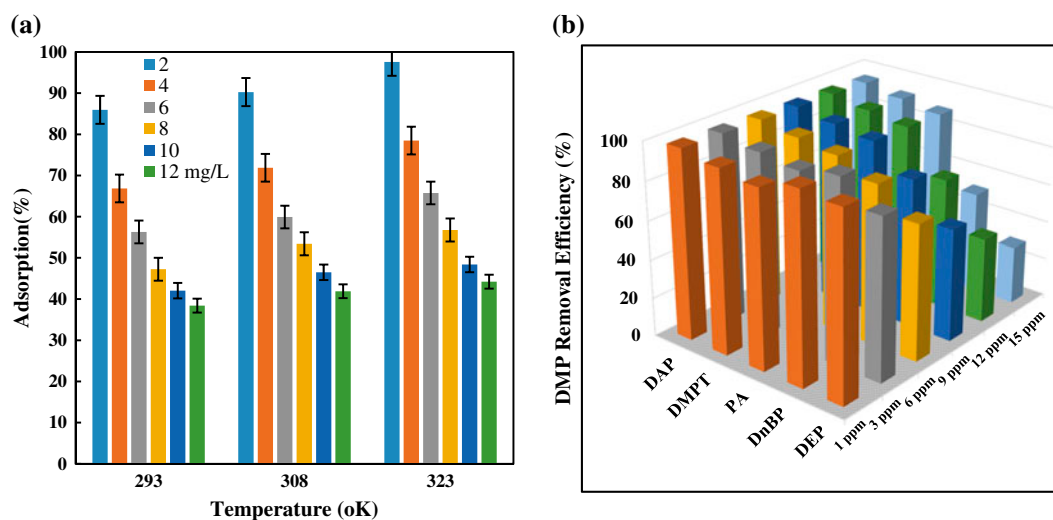


Fig. 7. (a) Effect of temperature on DMP adsorption using MZNC (Conditions: pH 3, adsorbent dose: 1 g/L and 20 min contact time and (b) effect of co-ester on DMP adsorption efficiency using MZNC.

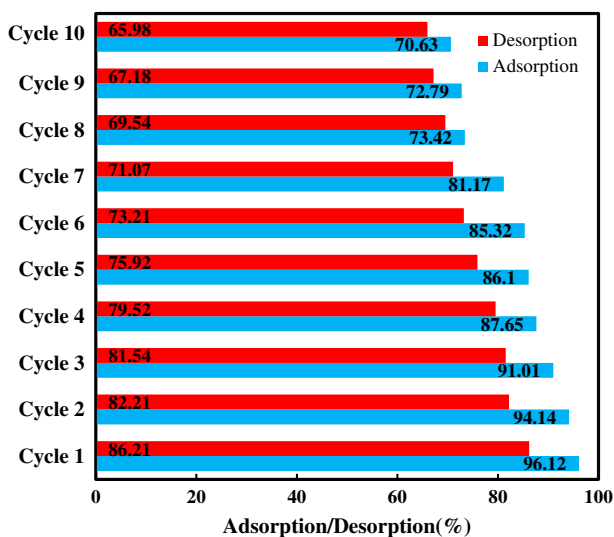


Fig. 8. Reuse (Adsorption/desorption) study of MZNC.

3.8. Interference of co-ester

Herein, the effect of foreign ester (e.g. DAP, DMPT, PA, DnPB, and DEP) as competing parameter on DMP adsorption efficiency was investigated. DMP concentration was kept at 8 mg/L and initial concentration of co-ester changed from 1 to 15 mg/L at room temperature so as to evaluate the effect of these compounds. Fig. 7(b) shows that DAP, DMPT, and PA have a very negligible effect on DMP removal process. However, the presence of DnPB and DEP substantially affect the removal process of DMP. As can be seen from the figure, when the DnPB and DEP concentration were increased from 1 to 15 mg/L, DMP sorption efficiency decreased by 46–66%, respectively. In other words, DnPB and DEP have a high propensity to compete with DMP to occupy the active adsorption site which will eventually lead to the decrease of DMP sorption percentage. This could be due to the high solubility of DnPB and DEP, compared to other compound, and their affinity toward the synthesized nanocomposite.

3.9. Desorption of DMP from MZNC

Desorption of DMP was also evaluated in a batch condition; the results are shown in Fig. 8. As shown in the figure, desorption capacity of DMP slightly reduced after the 10 consecutive cycles of sorption–desorption. Therefore, it can be speculated that MZNC is capable of being repeatedly applied for DMP adsorption without many losses in initial sorption capacities and its removal efficiency.

4. Conclusion

In this study, we synthesized MZNC as a hybrid adsorbent for removing DMP from aqueous solutions. The optimum conditions for DMP adsorption on MZNC were found to be at pH 3, contact time 20 min, Zeolite: Fe₃O₄ ratio molar of 2:1 and sorbent dosage 1 g/L and 50°C. The batch experiments indicated that the sorption process follows the Langmuir isotherm; and, kinetic data are also well-fitted with pseudo-second-order models. It was found that the adsorption of DMP is inherently endothermic and occurs spontaneously. In addition, DEP and DnBP significantly affected the removal of DMP by the synthesized adsorbent. We observed that the synthesized MZNC with high adsorption capacity and suitable magnetic properties is efficiently capable of removing DMP. Therefore, the synthesized adsorbent in this study can be applied as a promising adsorbent in the water and wastewater treatment.

Supplementary material

The Supplementary material for this paper is available online at <http://dx.doi.org/10.1080/19443994.2016.1178174>.

Acknowledgment

This work is supported by Tehran University of Medical Sciences and Iranian Nanotechnology Initiative Council.

References

- [1] K.M. Rodgers, R.A. Rudel, A.C. Just, Phthalates in food packaging, consumer products, and indoor environments, in: *Toxicants in Food Packaging and Household Plastics*, Springer, London, 2014, pp. 31–59.
- [2] S. Net, A. Delmont, R. Sempéré, A. Paluselli, B. Ouddane, Reliable quantification of phthalates in environmental matrices (air, water, sludge, sediment and soil): A review, *Sci. Total Environ.* 515–516 (2015) 162–180.
- [3] J. Wang, F. Wang, J. Yao, R. Wang, H. Yuan, K. Masakorala, M.M. Choi, Adsorption and desorption of dimethyl phthalate on carbon nanotubes in aqueous copper(II) solution, *Colloids Surf. A* 417 (2013) 47–56.
- [4] F. Yang, M. Wang, Z. Wang, Sorption behavior of 17 phthalic acid esters on three soils: Effects of pH and dissolved organic matter, sorption coefficient measurement and QSPR study, *Chemosphere* 93 (2013) 82–89.
- [5] M. Zolfaghari, P. Drogui, B. Seyhi, S. Brar, G. Buelna, R. Dubé, Occurrence, fate and effects of Di (2-ethylhexyl) phthalate in wastewater treatment plants: A review, *Environ. Pollut.* 194 (2014) 281–293.
- [6] L. Chang, P. Bi, X. Li, Y. Wei, Study of solvent sublimation for concentration of trace phthalate esters in plastic beverage packaging and analysis by gas chromatography–mass spectrometry, *Food Chem.* 177 (2015) 127–133.
- [7] E. Ahmadi, M. Gholami, M. Farzadkia, R. Nabizadeh, A. Azari, Study of moving bed biofilm reactor in diethyl phthalate and diallyl phthalate removal from synthetic wastewater, *Bioresour. Technol.* 183 (2015) 129–135.
- [8] Y. Gong, M. Gao, C. Sun, Study on biological effect of plasticizer, in: *Informatics and Management Science I*, Springer, London, 2013, pp. 679–684.
- [9] N. Adhoum, L. Monser, Removal of phthalate on modified activated carbon: Application to the treatment of industrial wastewater, *Sep. Purif. Technol.* 38 (2004) 233–239.
- [10] M. Qiao, W. Qi, H. Liu, J. Qu, Occurrence, behavior and removal of typical substituted and parent polycyclic aromatic hydrocarbons in a biological wastewater treatment plant, *Water Res.* 52 (2014) 11–19.
- [11] M. Julinová, R. Slavík, Removal of phthalates from aqueous solution by different adsorbents: A short review, *J. Environ. Manage.* 94 (2012) 13–24.
- [12] W. Jiang, J.A. Joens, D.D. Dionysiou, K.E. O’Shea, Optimization of photocatalytic performance of TiO₂ coated glass microspheres using response surface methodology and the application for degradation of dimethyl phthalate, *J. Photochem. Photobiol. A* 262 (2013) 7–13.
- [13] V. Boonyaraj, C. Chiemchaisri, W. Chiemchaisri, S. Theepharakspan, K. Yamamoto, Toxic organic micropollutants removal mechanisms in long-term operated membrane bioreactor treating municipal solid waste leachate, *Bioresour. Technol.* 113 (2012) 174–180.
- [14] B. Kakavandi, R.R. Kalantary, A.J. Jafari, S. Nasser, A. Ameri, A. Esrafil, A. Azari, Pb(II) adsorption onto a magnetic composite of activated carbon and superparamagnetic Fe₃O₄ nanoparticles: Experimental and modeling study, *CLEAN—Soil Air Water* 43 (2015) 1157–1166.
- [15] A. Mohseni-Bandpi, B. Kakavandi, R.R. Kalantary, A. Azari, A. Keramati, Development of a novel magnetite-chitosan composite for the removal of fluoride from drinking water: Adsorption modeling and optimization, *RSC Adv.* 5(89) (2015) 73279–73289.
- [16] N.A. Khan, B.K. Jung, Z. Hasan, S.H. Jhung, Adsorption and removal of phthalic acid and diethyl phthalate from water with zeolitic imidazolate and metal–organic frameworks, *J. Hazard. Mater.* 282 (2015) 194–200.

- [17] X. Luo, F. Zhang, S. Ji, B. Yang, X. Liang, Graphene nanoplatelets as a highly efficient solid-phase extraction sorbent for determination of phthalate esters in aqueous solution, *Talanta* 120 (2014) 71–75.
- [18] Q. Shi, A. Li, Q. Zhou, C. Shuang, Y. Li, Removal of diethyl phthalate from aqueous solution using magnetic iron-carbon composite prepared from waste anion exchange resin, *J. Taiwan Inst. Chem. Eng.* 45 (2014) 2488–2493.
- [19] W. Yan, L. Yan, J. Duan, C. Jing, Sorption of organophosphate esters by carbon nanotubes, *J. Hazard. Mater.* 273 (2014) 53–60.
- [20] S. Ait, B. Hamoudi, J. Hamdi, Z. Brendlé, Kessaissia, adsorption of lead by geomaterial matrix: Adsorption equilibrium and kinetics, *Sep. Sci. Technol.* 49 (2014) 1416–1426.
- [21] T.C. Nguyen, P. Loganathan, T.V. Nguyen, S. Vigneswaran, J. Kandasamy, R. Naidu, Simultaneous adsorption of Cd, Cr, Cu, Pb, and Zn by an iron-coated Australian zeolite in batch and fixed-bed column studies, *Chem. Eng. J.* 270 (2015) 393–404.
- [22] B. Szala, T. Bajda, J. Matusik, K. Zięba, B. Kijak, BTX sorption on Na-P1 organo-zeolite as a process controlled by the amount of adsorbed HDTMA, *Microporous Mesoporous Mater.* 202 (2015) 115–123.
- [23] H.-Y. Sun, L.-P. Sun, F. Li, L. Zhang, Adsorption of benzothiophene from fuels on modified NaY zeolites, *Fuel Process. Technol.* 134 (2015) 284–289.
- [24] M. Ansari, A. Aroujalian, A. Raisi, B. Dabir, M. Fathizadeh, Preparation and characterization of nano-NaX zeolite by microwave assisted hydrothermal method, *Adv. Powder Technol.* 25 (2014) 722–727.
- [25] A.A. Babaei, A. Azari, R.R. Kalantary, B. Kakavandi, Enhanced removal of nitrate from water using nZVI@MWCNTs composite: Synthesis, kinetics and mechanism of reduction, *Water Sci. Technol.* 72 (2015) 1988–1999.
- [26] P. Azizi, M. Golshekan, S. Shariati, J. Rahchamani, Solid phase extraction of Cu^{2+} , Ni^{2+} , and Co^{2+} ions by a new magnetic nano-composite: excellent reactivity combined with facile extraction and determination, *Environ. Monit. Assess.* 187 (2015) 1–11.
- [27] B. Kakavandi, A. Takdastan, N. Jaafarzadeh, M. Azizi, A. Mirzaei, A. Azari, Application of Fe_3O_4 @C catalyzing heterogeneous UV-Fenton system for tetracycline removal with a focus on optimization by a response surface method, *J. Photochem. Photobiol. A* 314 (2015) 178–188.
- [28] N. Jaafarzadeh, B. Kakavandi, A. Takdastan, R.R. Kalantary, M. Azizi, S. Jorfi, Powder activated carbon/ Fe_3O_4 hybrid composite as a highly efficient heterogeneous catalyst for Fenton oxidation of tetracycline: Degradation mechanism and kinetic, *RSC Adv.* 5 (2015) 84718–84728.
- [29] J.-Y. Tseng, C.-Y. Chang, Y.-H. Chen, C.-F. Chang, P.-C. Chiang, Synthesis of micro-size magnetic polymer adsorbent and its application for the removal of Cu(II) ion, *Colloids Surf. A* 295 (2007) 209–216.
- [30] L. Huang, Y. Sun, W. Wang, Q. Yue, T. Yang, Comparative study on characterization of activated carbons prepared by microwave and conventional heating methods and application in removal of oxytetracycline (OTC), *Chem. Eng. J.* 171 (2011) 1446–1453.
- [31] R. Rezaei Kalantry, A. Jonidi Jafari, A. Esrafil, B. Kakavandi, A. Gholizadeh, A. Azari, Optimization and evaluation of reactive dye adsorption on magnetic composite of activated carbon and iron oxide, *Desalin. Water Treatmt.* 57 (2015) 6411–6422.
- [32] G.D. Vuković, A.D. Marinković, S.D. Škapin, M.Đ. Ristić, R. Aleksić, A.A. Perić-Grujić, P.S. Uskoković, Removal of lead from water by amino modified multi-walled carbon nanotubes, *Chem. Eng. J.* 173 (2011) 855–865.
- [33] A.A. Babaei, A. Khataee, E. Ahmadpour, M. Sheydaei, B. Kakavandi, Z. Alaei, Optimization of cationic dye adsorption on activated spent tea: Equilibrium, kinetics, thermodynamic and artificial neural network modeling, *Korean J. Chem. Eng.* 33 (2015) 1–10.
- [34] A. Çelekli, G. İlgin, H. Bozkurt, Sorption equilibrium, kinetic, thermodynamic, and desorption studies of Reactive Red 120 on *Chara contraria*, *Chem. Eng. J.* 191 (2012) 228–235.
- [35] A. Azari, R.R. Kalantary, G. Ghanizadeh, B. Kakavandi, M. Farzadkia, E. Ahmadi, Iron-silver oxide nano-adsorbent synthesized by co-precipitation process for fluoride removal from aqueous solution and its adsorption mechanism, *RSC Adv.* 5 (2015) 87377–87391.
- [36] A. Azari, B. Kakavandi, R.R. Kalantary, E. Ahmadi, M. Gholami, Z. Torkshavand, M. Azizi, Rapid and efficient magnetically removal of heavy metals by magnetite-activated carbon composite: A statistical design approach, *J. Porous Mater.* 22 (2015) 1083–1096.
- [37] K. Li, Y. Zhang, Y. Dang, H. Wei, Q. Wang, Removal of Cr(VI) from aqueous solutions using buckwheat (*Fagopyrum esculentum* Moench) hull through adsorption-reduction: Affecting factors, isotherm, and mechanisms, *CLEAN-Soil Air Water* 42 (2014) 1549–1557.
- [38] M. Massoudinejad, A. Asadi, M. Vosoughi, M. Gholami, B. Kakavandi, M. Karami, A comprehensive study (kinetic, thermodynamic and equilibrium) of arsenic (V) adsorption using KMnO_4 modified clinoptilolite, *Korean J. Chem. Eng.* 32 (2015) 2078–2086.
- [39] B. Kakavandi, A. Jonidi Jafari, R. Rezaei Kalantary, S. Nasser, A. Ameri, A. Esrafil, Synthesis and properties of Fe_3O_4 -activated carbon magnetic nanoparticles for removal of aniline from aqueous solution: Equilibrium, kinetic and thermodynamic studies, *Iran J. Environ. Health Sci. Eng.* 10 (2013) 1–9.
- [40] E.T. Özer, B. Osman, A. Kara, N. Beşirli, Ş. Gücer, H. Sözeri, Removal of diethyl phthalate from aqueous phase using magnetic poly (EGDMA-VP) beads, *J. Hazard. Mater.* 229 (2012) 20–28.
- [41] C.-Y. Chen, C.-C. Chen, Y.-C. Chung, Removal of phthalate esters by α -cyclodextrin-linked chitosan bead, *Bioresour. Technol.* 98 (2007) 2578–2583.
- [42] W. Den, H.-C. Liu, S.-F. Chan, K.T. Kin, C. Huang, Adsorption of phthalate esters with multiwalled carbon nanotubes and its applications, *J. Environ. Eng. Manage.* 16 (2006) 275–282.
- [43] S.V. Mohan, S. Shailaja, M.R. Krishna, P. Sarma, Adsorptive removal of phthalate ester (Di-ethyl phthalate) from aqueous phase by activated carbon: A kinetic study, *J. Hazard. Mater.* 146 (2007) 278–282.

- [44] C.-Y. Chen, Y.-C. Chung, Removal of phthalate esters from aqueous solutions by chitosan bead, *J. Environ. Sci. Health Part A* 41 (2006) 235–248.
- [45] E.T. Özer, B. Osman, A. Kara, E. Demirbel, N. Beşirli, Ş. Güçer, Diethyl phthalate removal from aqueous phase using poly (EGDMA-MATrp) beads: Kinetic, isothermal and thermodynamic studies, *Environ. Technol.* 36 (2015) 1698–1706.
- [46] L. Yin, Y. Lin, L. Jia, Graphene oxide functionalized magnetic nanoparticles as adsorbents for removal of phthalate esters, *Microchim. Acta* 181 (2014) 957–965.
- [47] Z. Wang, Efficient adsorption of dibutyl phthalate from aqueous solution by activated carbon developed from phoenix leaves, *Int. J. Environ. Sci. Technol.* 12 (2015) 1923–1932.
- [48] B. Kakavandi, A. Esrafil, A. Mohseni-Bandpi, A.J. Jafari, R.R. Kalantary, Magnetic $\text{Fe}_3\text{O}_4@ \text{C}$ nanoparticles as adsorbents for removal of amoxicillin from aqueous solution, *Water Sci. Technol.* 69 (2014) 147–155.